Title

Photosynthetic efficiency predicts toxic effects of metal nanomaterials in phytoplankton

Journal

Aquatic Toxicology, 183

ISSN

0166445X

Authors

Miller, Robert J
Muller, Erik B
Cole, Bryan
et al.

Publication Date

2017-02-01

DOI

10.1016/j.aquatox.2016.12.009

Peer reviewed

Title:
Photosynthetic efficiency predicts toxic effects of metal nanomaterials in phytoplankton

Journal Issue:
AQUATIC TOXICOLOGY, 183

Author:
Miller, RJ
Muller, EB
Cole, B
Martin, T
Nisbet, R
Bielmyer-Fraser, GK
Jarvis, TA
Keller, AA
Cherr, G
Lenihan, HS

Publication Date:
02-01-2017

Series:
UC Santa Barbara Previously Published Works

Permalink:
http://escholarship.org/uc/item/4v59q4p3

DOI:
https://doi.org/10.1016/j.aquatox.2016.12.009

Keywords:
High throughput screening, Dynamic energy budget modeling, Plankton, Ecotoxicity, Metallic nanoparticles, Marine ecology

Local Identifier(s):
UCPMS ID: 1773269

Aquatic Toxicology 183 (2017) 85–93

Contents lists available at ScienceDirect

Aquatic Toxicology

journal homepage: www.elsevier.com/locate/aquatox

Research paper

Photosynthetic efficiency predicts toxic effects of metal nanomaterials in phytoplankton

Robert J. Miller[a,*,1], Erik B. Muller[a,1], Bryan Cole[b,1], Tyronne Martin[c], Roger Nisbet[d], Gretchen K. Bielmyer-Fraser[e], Tayler A. Jarvis[f], Arturo A. Keller[a], Gary Cherr[b,g], Hunter S. Lenihan[c]

[a] Marine Science Institute, University of California, Santa Barbara, CA, USA
[b] University of California Davis Bodega Marine Laboratory, University of California Davis, Bodega Bay, CA, USA
[c] Bren School of Environmental Science and Management, University of California Santa Barbara, CA, USA
[d] Department of Ecology Evolution and Marine Biology, University of California Santa Barbara, CA, USA
[e] Jacksonville University, Jacksonville, FL, USA
[f] Valdosta State University, Valdosta, GA, USA
[g] Department of Environmental Toxicology and Nutrition, University of California Davis, Davis, CA, USA

ARTICLE INFO

Article history:
Received 31 July 2016
Received in revised form 5 December 2016
Accepted 10 December 2016
Available online 23 December 2016

Keywords:
High throughput screening
Dynamic energy budget modeling
Plankton
Ecotoxicity
Metallic nanoparticles
Marine ecology

ABSTRACT

High Throughput Screening (HTS) using in vitro assessments at the subcellular level has great promise for screening new chemicals and emerging contaminants to identify high-risk candidates, but their linkage to ecological impacts has seldom been evaluated. We tested whether a battery of subcellular HTS tests could be used to accurately predict population-level effects of engineered metal nanoparticles (ENPs) on marine phytoplankton, important primary producers that support oceanic food webs. To overcome well-known difficulties of estimating ecologically meaningful toxicity parameters, we used novel Dynamic Energy Budget and Toxicodynamic (DEBtox) modeling techniques to evaluate impacts of ENPs on population growth rates. Our results show that population growth was negatively impacted by all four ENPs tested, but the HTS tests assessing many cell/physiological functions lacked predictive power at the population level. However, declining photosynthetic efficiency, a traditional physiological endpoint for photoautotrophs, was a good predictor of population level effects in phytoplankton. DEBtox techniques provided robust estimates of EC_{10} for population growth rates in exponentially growing batch cultures of phytoplankton, and should be widely useful for ecotoxicological testing. Adoption of HTS approaches for ecotoxicological assessment should carefully evaluate the predictive power of specific assays to minimize the risk that effects at higher levels of biological organization may go undetected.

1. Introduction

Novel chemicals and materials, including engineered nanomaterials, are being developed at an ever-increasing rate, but few are thoroughly evaluated for their potential to inflict harm to the environment. This is due in large part to traditional methods of ecotoxicological risk assessment that are time consuming and expensive. Accordingly, high-throughput screening (HTS) methods have been a promising approach for rapid risk assessment of new compounds, including nanomaterials (Nel et al., 2013; Knudsen et al., 2015). These approaches attempt to predict and explain responses of whole organisms and ecological systems by measuring responses at lower levels of biological organization, typically using in vitro assays to identify high-risk compounds and prioritize in vivo tests (Judson et al., 2013). The assays can also be used to identify mechanisms of cellular injury that can inform *in silico* models for predictive toxicology (Nel et al., 2013; George et al., 2011). Potential advantages include lower cost, less reliance on animal models, higher replication, and therefore greater confidence in results. HTS has proven highly useful in drug testing and human medical science (Nel et al., 2013). However, in ecotoxicology, most research has thus far focused on the in vitro level and relatively little has been done to evaluate the effectiveness of HTS methods in predicting higher-level ecological impacts.

* Corresponding author.
E-mail address: miller@msi.ucsb.edu (R.J. Miller).
[1] These authors contributed equally to this work.

http://dx.doi.org/10.1016/j.aquatox.2016.12.009
0166-445X/

HTS techniques measure cellular injury responses to toxicant exposure, e.g. fluorescent-probe-based proxies for mitochondrial membrane potential, intracellular calcium fluxes, and membrane permeability (George et al., 2010) that can be measured in high-capacity plate readers. Whether positive signals in HTS translate into impacts at higher levels of biological organization, where compensatory mechanisms may mitigate impacts, remains uncertain (Forbes and Calow, 2012). The need for HTS studies to be directly linked to organismal and population-level impacts is clear but has rarely been conducted. Phytoplankton offer a eukaryotic cell system where cellular/physiological endpoints can be rapidly assessed using an HTS approach, and organismal function (photosynthetic efficiency) and population-level growth can be readily determined.

Phytoplankton are single-celled planktonic photoautotrophs that are the dominant primary producers in the oceans. As small (0.2–200 μm) single or clustered cells with high surface-to-volume ratios suspended in water, they are vulnerable to pollution, especially in coastal zones where they are abundant (Lucas et al., 2011) and contaminants may be concentrated (Bowen and Depledge, 2006). Impacts to phytoplankton may cascade through marine food webs, since reductions in population growth rate of phytoplankton cells reduce resources available for consumers (Edwards and Richardson, 2004), and accumulation of contaminants in phytoplankton can lead to trophic transfer and consequent toxic effects on consumers (Hanna et al., 2013a; Bielmyer-Fraser et al., 2014). Metals are a common class of contaminants that impact phytoplankton and accumulate in coastal marine food webs, and metallic nanomaterials are an emerging form of metal contamination in coastal marine ecosystems (Gottschalk et al., 2009; Gottschalk et al., 2013). Nanomaterials are widely employed for their enhanced mechanical, optical, and electromagnetic properties relative to larger forms of similar materials (Pitkethly, 2004). Engineered nanoparticles (ENPs) are nanomaterials created with all three dimensions at the nanoscale (1–100 nm). Because of their adoption in wide array of applications, including electronics, chemistry, cosmetics, and biomedicine (West and Halas, 2003; Mauter and Elimelech, 2008; Barreto et al., 2011), ENPs and other nanomaterials are emerging as a new class of contaminants, with potentially negative environmental consequences (Klaine et al., 2008). Metal-based nanomaterials in particular are commonly used because they are synthesized relatively easily and have myriad industrial and consumer applications (Rao et al., 2004). As the volume of nanomaterials production and subsequent discharge into the marine environment increases, so does the potential for wide-ranging ecological impacts (Knudsen et al., 2015). Exposure of aquatic organisms to nanomaterials is difficult to quantify, but modeling efforts have estimated concentrations of metal oxide ENPs in aquatic systems at levels of significant concern (Gottschalk et al., 2009; Gottschalk et al., 2013).

Here we investigate the potential of four fluorescence-based HTS assays of cellular health to predict population-level impacts of ZnO, Ag, CeO and CuO ENPs, specifically the population growth rate of a geographically widespread prymnesiophyte phytoplankton species, *Isochrysis galbana*. The HTS assays are designed to measure different aspects of cellular functioning and integrity, including mitochondrial membrane potential, occurrence of reactive oxygen species (ROS), cellular efflux pump activity and cell membrane permeability. Since photosynthetic processes are well-known targets of metal toxicity (Clijsters and Vanassche, 1985), we also used a non-HTS, physiological assay to measure impacts on photosynthetic efficiency. Cell densities measured during the exponential growth phase in batch cultures were analyzed within a Dynamic Energy Budget and Toxicodynamic (DEBtox) modeling framework to determine impacts of ENPs on population growth rates. Building on models we used previously (Muller et al., 2010; Miller et al., 2010), we developed new formalism to obtain robust estimates of EC_{10} for population growth rates exposed to the suite of commonly used metallic ENPs.

2. Materials and methods

All the ENPs used were characterized for the central materials library maintained by University of California's Center for Environmental Implications of Nanotechnology (UC CEIN)(Godwin et al., 2009). ZnO and CeO_2 ENPs were obtained from Meliorum Technologies (Rochester, NY, USA) and characterized for size, morphology, and chemical composition (Montes et al., 2012). Briefly, the primary ZnO ENPs were spheroid with a mean dry diameter of 24 ± 3 nm and a surface area of 42.1 $m^2\ g^{-1}$. Their agglomerate hydrodynamic diameter was 205 ± 14 nm in nanopure water (18.2 MΩ cm). The primary CeO_2 ENPs were rods ($67 \pm 8 \times 8 \pm 31$ nm) with a surface area of 93.8 $m^2\ g^{-1}$ and an agglomerate hydrodynamic diameter of 231 ± 16 nm in NanoPure water. CuO ENPs were obtained from Sigma-Aldrich (St. Louis, MO, USA) and described as < 50 nm and 99.8% pure; characterization with ICP-OES and TEM showed that they were 84.8 ± 2.7% pure (impurities included Na, Ca, Si, and Mg) and 20–100 nm in diameter (Hanna et al., 2013b). AgO ENPs were obtained from QuantumSphere Inc. (Santa Ana, CA) and described as 20–30 nm in diameter. TEM characterization showed that the AgO ENPs were 20–70 nm in diameter; no detectable impurities were found (Bielmyer-Fraser et al., 2014). The behavior in seawater of all particles used in this study has been previously characterized and is summarized in Table 1. All aggregate significantly in seawater. ZnO dissolves rapidly, whereas CuO and Ag dissolve very slowly and CeO dissolution was undetectable (Table 1).

2.1. Phytoplankton culture

Axenic cultures of *Isochrysis galbana* were obtained from the Provasoli-Guillard National Center for Culture of Marine Phytoplankton (Bigelow Laboratory for Ocean Sciences, West Boothbay Harbor, Maine, USA), and were maintained in standard media (f/2) made with filtered (0.22 μm filtered) natural seawater, which was autoclaved prior to inoculation. For cellular metal accumulation measurements, phytoplankton were cultured in synthetic seawater made by mixing Instant Ocean salt with 18 mΩ Milli-Q water and aerating at least 24 h before use. To provide inoculant for experiments, algae were incubated in polycarbonate flasks under cool white fluorescent lights (14:10 light:dark, 100–120 μmol $m^{-2}\ s^{-1}$) at 20 °C with aeration for 5–7 d, until log phase growth prevailed. Cell densities were measured directly by hemacytometer (Reichert, NY, USA) at 200× magnification or using a fluorometer (Turner Trilogy) calibrated with hemacytometer data.

2.2. ENP preparation and dispersion

ENP dispersions were prepared within 45 min of the start of each experiment. ENP stock suspensions were prepared by adding 10 mg of metal oxide ENPs to 10 mL of ultrapure 18 mΩ Milli-Q water, vortexing for 30 s, sonicating for 45 min, and adding 100 μL of 2 mg L^{-1} alginate (previously made stock in 18 mΩ Milli-Q water), and vigorously vortexing again for 1 min.

2.3. Phytoplankton population growth

All experiments were conducted at 20 °C, 34 ppt salinity, under the same illumination schedule described above. All glassware was acid-washed, rinsed with purified water (Barnstead nanopure, resistivity >18 MΩ cm), and autoclaved before use. Experiments were run in 125 mL polycarbonate flasks, media volume 50 mL, and were mixed at ~150 rotations per min on a rotary shaker (New Brunswick Scientific Co., NJ, USA). ENP concentrations tested were

Table 1
Engineered nanoparticle (ENP) characteristics in seawater. Particle aggregate diameters all plateaued within 30 min of the start of the measurements. Dissolution rates were measured for 10 mg L^{-1} solutions. Data are means with standard error. See references for more detail. * = A. Keller, unpublished data.

ENP	ENP aggregate diameter (nm)	Dissolution rate (percent day^{-1})	Zeta potential (mV)
ZnO	440.2 ± 65 (Keller et al., 2010)	27.2 ± 9% (Keller et al., 2010)	−0.51 ± 3.3 (Miller et al., 2010)
CeO_2	858.1 ± 75 (Keller et al., 2010)	Nd (Priester et al., 2014)	−0.64 ± 3.1 (Keller et al., 2010)
CuO	294.9 ± 12 (Hanna et al., 2013b)	0.05 ± 0.01% (Hanna et al., 2013b)	−12.7 ± 1.9*
Ag	593 ± 170 (Thio et al., 2011)	3.0% ± 0.7 (Thio et al., 2011)	−13.1 ± 1.3*

0, 0.25, 0.5, 1, 2.5, and 5 mg L^{-1} for ZnO (0, 3.07, 6.14, 12.29, 30.72, and 61.43 μM) and CuO (0, 3.14, 6.29, 12.57, 31.43, and 62.85 μM), and 0, 1, 2.5, 5, 7.5 and 10 mg L^{-1} for Ag (0, 9.27, 23.18, 46.35, 69.53, and 92.70 μM) and CeO (0, 5.81, 14.53, 29.05, 43.58, and 58.10 μM). Concentration ranges were based on pilot experiments and previous work showing the range of effects on phytoplankton. Five replicates were measured per treatment. Flasks were inoculated with 1–2 × 10^5 cells ml^{-1}, and cell densities were monitored every 24 h for 96 h.

2.4. Cellular screens

Smaller cultures for cellular assays were inoculated in 50 mL polycarbonate tubes. We added 100 μL of 2 mg L^{-1} alginate to each tube, along with a volume of filtered seawater and algal culture so that the addition of freshly prepared 1 mg L^{-1} ENP stock, enough to achieve the indicated final ENP concentration, would give 15 mL final volume. The tubes were placed under 12:12 light:dark cycle on an orbital shaker moving at 45 rotations per min. A 4.5 mL aliquot was taken from each exposure container 24 h after ENP addition, and again every 24 h thereafter, and used in the cellular screening to assess response to ENP exposure.

2.5. High throughput screens (HTS)

Four fluorescence-based assays for different aspects of cellular health were run on ENP-exposed phytoplankton and controls. The probes evaluated mitochondrial membrane potential (JC1, excitation λ 485 nm, emission 535/630 nm), reactive oxygen species or ROS (DCF, excitation λ 485 nm, emission 535 nm), cellular efflux pump inhibition (Calcein AM [CAM], excitation λ 485 nm, emission 535 nm), and membrane permeability (EHD, excitation λ 535 nm, emission 630 nm). Phytoplankton HTS were performed in black polycarbonate, clear bottom 96-well plates. After taking the subsample of ENP-exposed algae for a given time point, 200 μL per well of the sample was added to 2 columns (16 wells total) of the 96-well plate for each concentration. As there were 5 ENP concentrations plus the control, this completely filled a 96-well plate. Each probe treatment was replicated in 4 wells for each ENP concentration. In cases where probe fluorescence wavelengths were non-overlapping, multiple probes were combined. Following distribution of the samples into the 96-well plate, probes were added, the plate was mixed gently, and then incubated at 15 °C for 45 min. Final probe concentrations were: 0.2 μg mL^{-1} JC1, 1.0 μM DCF, 0.5 μM CAM, and 0.2 μM EHD. All probe stocks were dissolved in DMSO and stored in single-experiment aliquots at −20 °C. After incubation, fluorescence measurements were made at the appropriate wavelengths using a Tecan GENios microplate reader (Maennedorf, Switzerland). Each ENP exposure was replicated at least 4 times, and each probe/ENP combination was replicated 4 times within each experiment. This process was repeated for the 24, 48 and 72 h time points.

2.6. Photosynthetic efficiency

Chlorophyll fluorescence kinetics were measured with a Pulse Amplitude Modulated fluorometer (WATER PAM, Heinz Walz, Germany). At the end of the 96 h growth experiments, 4 mL aliquots of each replicate culture were dark-adapted for 15 min, after which saturating light pulses (800 ms, 3000 μmol m^{-2} s^{-1}) were given to induce maximal fluorescence yield, Fm, and maximal variable fluorescence, Fv, such that ΔF/Fm = Fv/Fm is maximal. Fv/Fm was used as a measure of the potential quantum yield of photosystem II (PS II). Calculations were made using Wincontrol software (v 3.18).

2.7. Metal distribution in algae

To examine potential cellular accumulation of ENPs in phytoplankton, *I. galbana* were cultured as described above, using f/2 media without trace metals and without ethylenediaminetetraacetic acid (EDTA). *I. galbana* was exposed to ZnO, Ag, and CuO nanoparticles for 72 h at the following nominal concentrations: 0.25 and 5 mg L^{-1} (3.07 and 61.43 μM) ZnO, 1 and 10 mg L^{-1} (9.27 and 92.70 μM) Ag, and 0.25 and 5 mg L^{-1} (3.14 and 62.85 μM) CuO. CeO_2 exposures were also conducted but are not presented here due to loss of samples in shipping that led to inadequate data. There were three replicate flasks per treatment, and a control treatment was included in each experiment. Approximately 5 × 10^8 cells L^{-1} were added to each flask at the start of the experiments. Following the algal inoculation, water samples were collected in 15 mL polypropylene centrifuge tubes for subsequent metal analysis. Cultures were continuously aerated with sterile 1 mL pipettes and stirred once d^{-1} by swirling. At the end of the exposure period, the algae cells were concentrated by centrifugation in 50 mL polypropylene centrifuge tubes at 3500 rpm for 15 min. Subsamples of the concentrated algae were collected for dry weight measurement and metals analysis. Algae was filtered and washed with 0.5 M ammonium formate to eliminate salts, and dry weights were determined by drying 1 mL of algae from each treatment in pre-weighed aluminum weigh boats in an oven at 80 °C for 1 d.

The intact algal cells from each treatment were washed with a metal chelator, 0.01 M EDTA, and then centrifuged at 3500 rpm for 15 min. The supernatant fractions, representing loosely bound metals on the algal surface, were collected in 15 mL centrifuge tubes. The remaining algal pellets were resuspended in 1 mL of purified 18 mΩ Milli-Q water and sonicated for approximately 1 min to lyse the cells, which was verified using a light microscope. The sample was then differentially centrifuged to separate the cells into cell wall, organelle, endoplasmic reticulum, and cytosol fractions. Lysed cells were centrifuged at 4000 rpm for 15 min to obtain the cell wall fraction. The organelle fraction was then obtained by centrifuging the remaining supernatant for 30 min at 10,000 rpm. The supernatant was then centrifuged at 100,000 rpm for 1 h to obtain the total membrane fraction (endoplasmic reticulum). The remaining supernatant represented the cytosol fraction. Each fraction was digested by addition of 1 mL of trace metal grade nitric acid (Fisher Scientific, Pittsburgh, PA) and 1 mL of purified 18 mΩ Milli-Q water and analyzed for metal concentration as described below.

2.8. Metal analysis

Digested algae fractions and filtered (0.45 μm) water samples were acidified with trace metal grade nitric acid (Fisher Scientific, Pittsburgh, PA), diluted with 18 mΩ Milli-Q water, and analyzed for metal concentration using graphite furnace atomic absorption spectrophotometry (GFAAS; Perkin-Elmer, AAnalyst 800). Samples were analyzed in triplicate, and metal standard solutions were analyzed after every ten samples for QC/QA purposes. Detection limits for metals were 1 $\mu g\,L^{-1}$.

2.9. DEBtox models

Dynamic Energy Budget (DEB) and toxicodynamic (TD) models are detailed in the Supplemental Information; this section presents model equations that were needed for parameter estimation. In the exponential growth phase of algal cell cultures, the cell density at time t and exposure concentration C, $N_{t,C}$, is

$$\ln N_{t,C} = \ln N_{0,C} + r_C t \tag{1}$$

with r_C as the population growth rate in the presence of toxicants. With sublethal toxic effects on assimilation (i.e. resource processing) and maintenance (i.e. the energy needs of a cell to remain viable),

$$r_C = \frac{r_0}{f_E}\left(1 - \frac{(1 - x f_{EX})(f_E f_M - 1)}{(f_{EX} f_{MX} - 1)}\right) \tag{2}$$

in which r_m is the maximum population growth rate (i.e. with abundant resources and without toxicants); and x is the population growth rate at an EC_X of choice as a fraction of r_0 (this study seeks to estimate EC_{10}, i.e. $x = 0.9$). The TD model equations for toxic effects on assimilation and maintenance, respectively f_E and f_M, are

$$f_E = 1 + \frac{(C - C_{E0})_+}{C_{Ek}} \tag{3}$$

and

$$f_M = 1 + \frac{(C - C_{M0})_+}{C_{Mk}} \tag{4}$$

with C_{*0} and C_{*k} as the no-effect concentration and the toxic effect scaling parameter for assimilation (* representing *'E'*) and maintenance (* representing *'M'*), respectively (the subscripted '+' indicates that $C - C_{*0} = 0$ if $C \le C_{*0}$). f_{EX} and f_{MX} are the functional values of f_E and f_M when the exposure concentration equals EC_X.

Generally, growth data alone do not contain sufficient information for estimating all model parameters in Eqs. (1)–(4). Accordingly, following Muller et al., (Muller et al., 2010), three special cases were assumed:

1 $C_{E0} = C_{M0} \equiv C_0$ and $C_{Ek} = C_{Mk} \equiv C_k$, thus $f_{EX} = f_{MX}$ and $f_E = f_M$; this will be referred to as the effect on maintenance and assimilation TD (MATD) model, which has 5 free parameters.
2 $C_{M0} \gg C$, thus $f_{MX} = f_M = 1$; this is the effect on assimilation only TD (ATD) model, which also has 5 free parameters.
3 $C_{E0} \gg C$, thus $f_{EX} = f_E = 1$; this is the effect on maintenance only TD (MTD) model, which has 4 free parameters.

In the latter two special cases, Eq. (2) simplifies considerably (see Supplemental Information). In the MTD model, the population growth rate is a simple linear function of the exposure concentration, which does not include the toxicant scaling parameter C_{Mk} (see Eq. SI.12).

Parameters of the DEB model were estimated from growth curves of cell densities (calculated form chlorophyll content) by maximizing the likelihood function assuming additive log normally distributed error. Each individual measurement during the exponential growth phase was included in the calculation of likelihood and parameters were simultaneously estimated from data of all treatments (per ENP), implying that 4 or 5 parameters were estimated from 8 or 9 growth curves. Confidence intervals of estimates were determined using likelihood profiles. Likelihood ratio tests were used to determine whether no-effect concentrations differed significantly from 0 (at the 95% level).

3. Results

3.1. Population growth

All four ENPs negatively impacted the population growth of *I. galbana* in batch cultures (Fig. 1, Fig. S1). The impact of exposure to CeO_2 and CuO ENPs at or below 20 $mg\,L^{-1}$ (116.2 μM CeO_2, 251.4 μM CuO) was relatively modest, whereas Ag had a stronger negative impact on population growth. ZnO ENPs proved to be the most toxic, probably because they dissolve relatively rapidly. With exposure levels beyond 1 $mg\,L^{-1}$ (12.29 μM) ZnO ENPs, cell densities even declined, indicating that mortality was a major toxic effect in these cultures.

The three TD models described in the Models Section were fitted to cell densities measured during the exponential growth phase (Fig. S1). Except for the MATD and ATD model fitted to cells exposed to ZnO ENPs, all estimates for no-effect concentrations did not differ significantly from 0 (results not shown). Accordingly, in those cases, no-effect concentrations were set at 0 while estimating other parameter values (Table S1).

Based on calculated log likelihood values (Table S1), the MTD model performed particularly poorly in fitting cell densities in cultures exposed to Ag and ZnO ENPs. The ATD model provided superior fits to these data sets. In contrast, all TD models fitted exponential growth in the presence of CuO ENPs about equally well. Since the MTD has one free parameter less than the other two TD models, it is the best fitting model at the 95% confidence level of growth data with CuO. However, it should be noted that estimates of parameter values differ relatively little among TD model variants. In this case, the estimates of the parameter that is particularly relevant for this study, the EC_{10}, differ 14% between the MTD and ATD models; this difference is statistically insignificant at the 95% confidence level (Table S1).

Data from cultures exposed to CeO_2 ENPs proved to be problematic for the MATD and ATD models. The toxicant scaling parameters in these models, C_k and C_{Ek} respectively, drifted to very large values while marginally improving the fit during the estimation procedure. Due to the relatively mild toxicity of CeO_2 ENPs, the MATD and ATD models became nearly linear functions of the CeO_2 exposure concentration (Equation S13). Thus, these models were effectively reduced to a functional form identical to the MTD model.

In sum, the ATD model was globally the best performing model, with the exception of its inability to capture the CeO_2 exposure data. Therefore, parameter estimates obtained with the ATD model are used in analyses below, except for parameter values estimated from CeO_2 exposed cultures, for which the estimates from the MTD model are used (Table 2). Population growth rates calculated with those parameter estimates reveal the large difference in impact potential among ENPs; Fig. 1 shows those population growth rates scaled to the maximum population growth rate estimated for each respective material. The scaled population growth rate declines rapidly and in a highly nonlinear fashion with increasing ZnO ENP concentrations. A similar but less pronounced trend is observed with the Ag ENPs. In contrast, with the same concentration range, CeO_2 and CuO ENPs have a milder impact on the (scaled) population growth rate. This impact appears to be nearly linear; a more

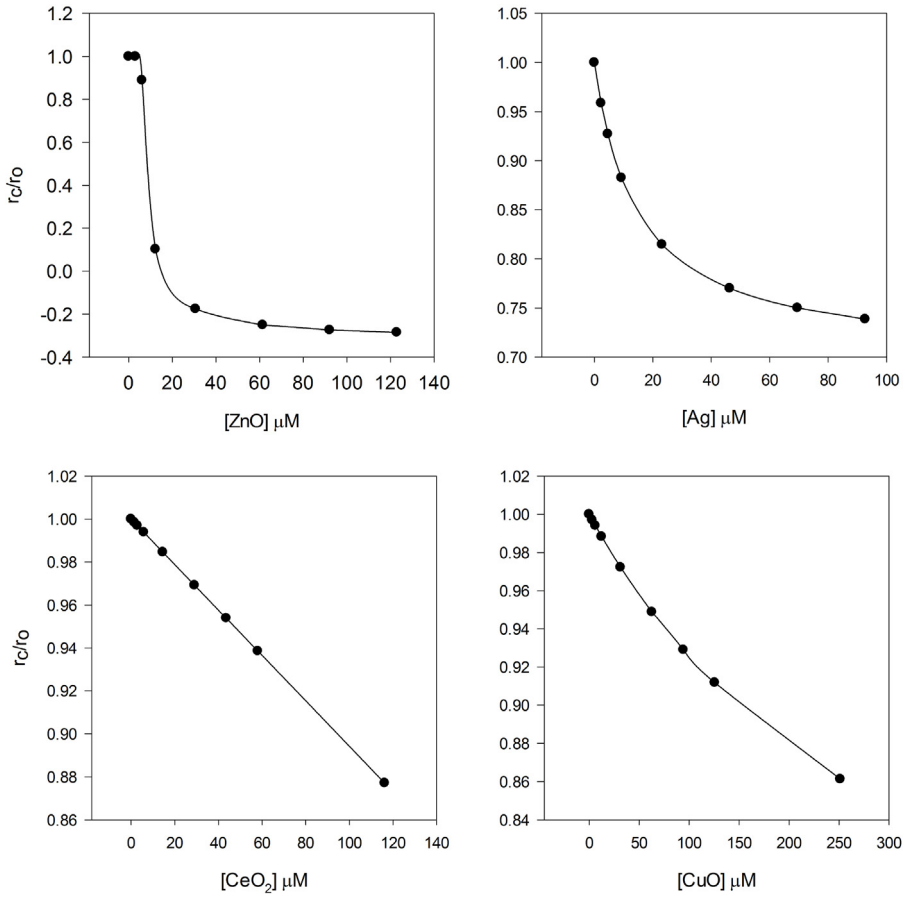

Fig. 1. Population growth of *Isochrysis galbana* in response to increasing concentration of metal oxide engineered nanoparticles (ENP) expressed relative to control cultures. Growth is estimated from cell count data using DebTox models described in Methods.

pronounced nonlinear response may be expected at exposure concentrations higher than applied in the experiments of this study.

3.2. Subcellular assays

The four assays of cellular health displayed variable and inconsistent responses to metal oxide ENP exposure, and in most cases no clear pattern was observed in the timing of the responses, which were measured after 24, 48, and 72 h of exposure. Membrane permeability, a proxy for cell death, clearly increased at relatively low concentrations of ZnO and CeO (Fig. S2). For ZnO, this trend was apparent in all time points, but the increase was greatest at 72 h. For CeO, a significant increase was seen only at 24 h (Fig. S2). No significant increase in membrane permeability was seen in response to exposure to CuO or Ag, except at 10 mg L^{-1} (92.7 μM) Ag, and only then at the 24 h.

Mitochondrial membrane potential declined after 72 h of ZnO exposure (Fig. S3). This pattern was evident but weaker at 48 h and not apparent at 24 h, except at 5 mg L^{-1} (61.4 μM) ZnO concentration. In contrast, mitochondrial membrane potential showed apparent increases after 72 h of exposure to CeO and Ag. No other clear patterns of response were seen for this variable.

Intracellular ROS levels also showed few clear patterns in response to metal oxide ENP exposure (Fig. S4). ROS increased with CuO exposure, with the largest increase at 72 h. In contrast, ROS levels dropped in response to ZnO exposure, although this response was not significant until 5 mg L^{-1} (61.4 μM) ZnO concentration. No pattern in ROS levels was seen in response to CeO or Ag exposure.

Accumulation of calcein AM (CAM) in cells is an indicator of inhibition of multidrug efflux transporters (ABC family transporters), with increased values suggesting a decrease of this important mechanism of cellular defense. CAM fluorescence clearly increased in response to ZnO exposure, with no clear differences between time points (Fig. S5). A smaller relative increase was seen in response to CeO exposure, and it was clearest after 72 h. Similarly, CAM increased slightly at 72 h in response to Ag exposure but no pattern was apparent at earlier time points. For CuO, an increase was also evident at 72 h but only for lower exposure concentrations up to 2.5 mg L^{-1} (31.4 μM).

Table 2
DEB and TD model parameter values; estimated values include 95% confidence intervals in parentheses.

ENP	N_0	r_0	EC_{10}	C_{E0}	C_{Ek}
	cells μl^{-1}	day^{-1}	μM	μM	μM
Ag	32.9 (30.6–35.3)	1.26 (1.22–1.31)	7.23 (4.91–10.8)	0	14.7 (9.46–24.0)
CeO_2	31.2 (29.1–33.5)	0.97 (0.95–1.00)	94.5 (74.4–131)	0	–
ZnO	43.8 (31.1–61.8)	0.66 (0.54–0.78)	6.11 (5.53–7.49)	5.87 (5.16–7.37)	3.00 (1.23–5.90)
CuO	6.56 (5.95–7.23)	1.31 (1.27–1.35)	150 (96.1–231)	0	337 (80->1e4)

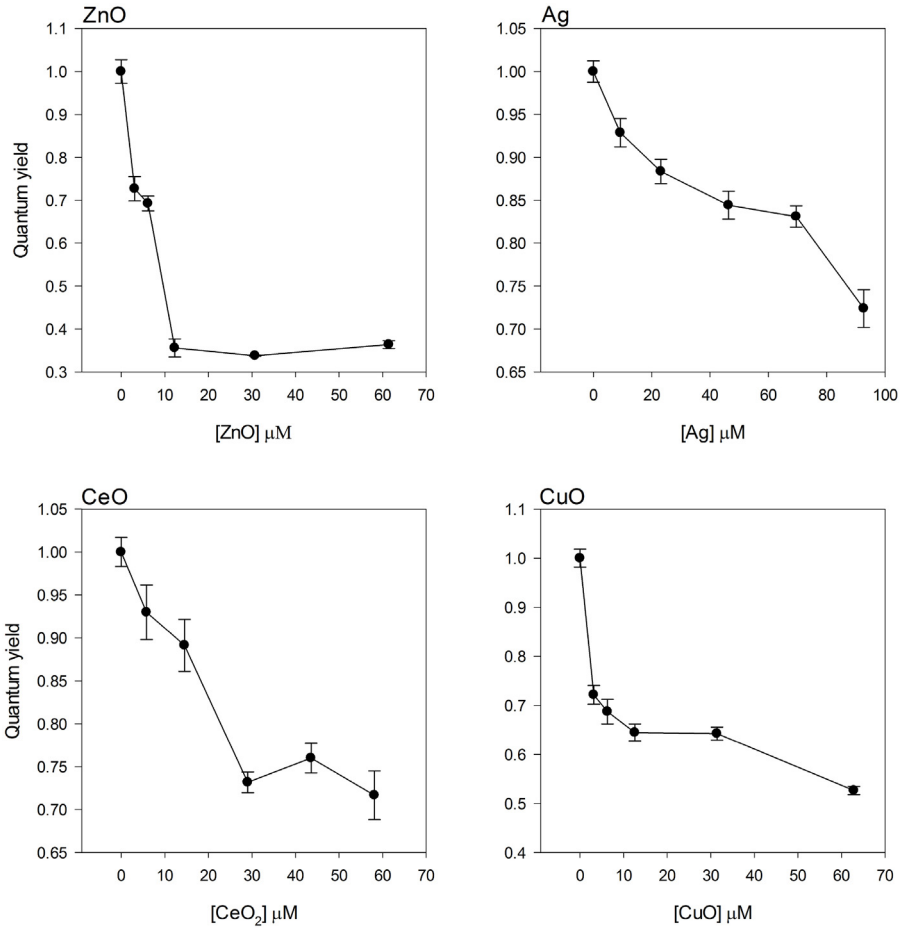

Fig. 2. Photosynthetic yield of *Isochrysis galbana* measured as variable fluorescence divided by maximum fluorescence (Fv/Fm) in response to increasing concentration of metal oxide ENPs, expressed relative to control cultures.

3.3. Photosynthetic efficiency

The efficiency (yield) of photosystem II, measured via pulse amplitude modulated (PAM) fluorometry, showed clear decreases matching responses in population growth rate (Fig. 2). ZnO exposure elicited the strongest response, with photosynthetic yield declining by ~60% compared to control values at 1 mg L^{-1} (12.3 μM) ZnO (Fig. 2). The response to CuO exposure was also strong, with a decline of ~30% at the lowest concentration of 0.25 mg L^{-1} (3.14 μM). Less precipitous, but clear declines were seen in response to exposure to CeO and Ag, with both exposures resulting in ~30% declines in yield at the highest concentrations (Fig. 2).

3.4. Subcellular ENP accumulation

Zinc oxide clearly penetrated the phytoplankton cells. At both the 0.25 mg L^{-1} (3.07 μM) and 5 mg L^{-1} (61.4 μM) exposure levels, zinc levels were nearly split between the fractions representing the exterior of the cell (EDTA wash and cell wall) and the interior (cytosol, organelles and endoplasmic reticulum). On average, 54.5% of the cellular-associated Zn was in the exterior fractions versus 45.3% interior (Table 3). This contrasted with the results for Ag, where 79.2% of the metal was found in the exterior versus 20.1% interior. There was no evidence for cellular accumulation of Cu at either exposure level: Cu concentrations in all fractions were similar to controls (Table 3).

4. Discussion

Photosynthetic efficiency, expressed as maximum quantum yield of photosystem II, was a sensitive indicator of population-level toxicity of ENPs to phytoplankton. This result is not particularly surprising given the overwhelming importance of photosynthesis to algal cells and what we know about the toxicity of metals to the photosynthetic process (Clijsters and Vanassche, 1985). What was unexpected was the unreliability of more typical cellular HTS assays as early warning indicators or predictors of toxicity at the population level. For phytoplankton, therefore, these specific assays should not be relied on for ecotoxicological risk assessment at present. Instead the more traditional growth experiments combined with photosynthesis measurements are currently more accurate and effective measures of potential impact of ENPs to this important group of organisms (Fig. 3).

Trace metals like Zn and Cu are at very low concentrations in nature, and they are often biochemically utilized by organisms including phytoplankton. For example, Zn has a key role for enzymatic catalysis, while Cu mediates redox transformations (Merchant, 2010). Thus, algal cells have a high uptake affinity for these nutrient metals, which helps them to take advantage of pulsed inputs, such as iron windfalls from large desert dust storms (Sunda and Huntsman, 1995; Marchetti et al., 2009). This high affinity promotes some non-specificity of cellular nutrient metal transport systems, such that other reactive metals, including Cu and Cd, can enter cells via the transport systems for nutrient metals such as Mn and Zn (Sunda and Huntsman, 1996; Sunda and

Table 3
Mean metal concentrations in cellular fractions of *Isochrysis galbana* exposed to two concentrations of ENPs for 72 h. Units are μg metal per cell; standard deviations are in parentheses. EDTA wash fraction represents metals loosely bound to cell exterior. ER = endoplasmic reticulum.

Fraction	ZnO			Ag			CuO		
	control	0.25 mg L^{-1}	5 mg L^{-1}	control	1 mg L^{-1}	10 mg L^{-1}	control	0.25 mg L^{-1}	5 mg L^{-1}
EDTA wash	$7.67E^{-12}$ ($2.69E^{-13}$)	$2.64E^{-10}$ ($3.84E^{-11}$)	$5.97E^{-10}$ ($1.02E^{-10}$)	$2.08E^{-10}$ ($2.18E^{-12}$)	$5.84E^{-10}$ ($7.55E^{-11}$)	$6.94E^{-10}$ ($2.70E^{-11}$)	$2.28E^{-10}$ ($9.13E^{-13}$)	$2.32E^{-10}$ ($4.98E^{-11}$)	$4.60E^{-10}$ ($1.75E^{-11}$)
Cell wall	$1.43E^{-11}$ ($2.59E^{-13}$)	$4.03E^{-10}$ ($1.10E^{-11}$)	$5.97E^{-10}$ ($1.02E^{-10}$)	$1.89E^{-10}$ ($2.76E^{-12}$)	$7.22E^{-10}$ ($5.72E^{-11}$)	$1.10E^{-9}$ ($6.71E^{-11}$)	$1.73E^{-10}$ ($2.52E^{-12}$)	$1.17E^{-10}$ ($8.67E^{-11}$)	$3.73E^{-9}$ ($4.42E^{-11}$)
Cytosol	$8.33E^{-12}$ ($5.47E^{-13}$)	$7.59E^{-10}$ ($1.11E^{-11}$)	$5.97E^{-10}$ ($1.02E^{-10}$)	$7.82E^{-11}$ ($8.11E^{-13}$)	$1.31E^{-11}$ ($9.64E^{-12}$)	$2.82E^{-10}$ ($1.16E^{-10}$)	$8.78E^{-11}$ ($1.78E^{-13}$)	$9.79E^{-11}$ ($2.56E^{-12}$)	$2.84E^{-10}$ ($1.34E^{-10}$)
Organelles	$7.84E^{-12}$ ($2.04E^{-13}$)	$2.58E^{-10}$ ($2.38E^{-11}$)	$5.97E^{-10}$ ($1.02E^{-10}$)	$8.10E^{-11}$ ($1.24E^{-12}$)	$1.21E^{-10}$ ($3.46E^{-11}$)	$2.17E^{-10}$ ($7.37E^{-11}$)	$6.68E^{-11}$ ($2.03E^{-12}$)	$1.88E^{-10}$ ($1.19E^{-10}$)	$7.30E^{-10}$ ($6.70E^{-11}$)
ER	$7.09E^{-12}$ ($7.70E^{-13}$)	$2.26E^{-10}$ ($7.30E^{-11}$)	$5.97E^{-10}$ ($1.02E^{-10}$)	$6.72E^{-11}$ ($2.60E^{-12}$)	$6.87E^{-11}$ ($2.41E^{-11}$)	$2.04E^{-10}$ ($7.74E^{-11}$)	$8.15E^{-11}$ ($4.06E^{-12}$)	$7.30E^{-11}$ ($6.70E^{-11}$)	$1.70E^{-10}$ ($1.03E^{-10}$)

Fig. 3. Relationship of declines in photosynthetic yield (measured as Fv/Fm) to population growth (estimated as r_c/r_o) for *Isochrysis galbana* across all exposures to metal oxide ENPs. ZnO is graphed separately in panel B for clarity. Lines are least squares linear regression fits for each material (Ag: % decline $r_c/r_o = 1.533^*$ fv/fm, $r^2 = 0.77$, CeO_2: % decline $r_c/r_o = 0.171^*$ fv/fm, $r^2 = 0.84$, ZnO: % decline $r_c/r_o = 0.581^*$ fv/fm, $r^2 = 0.84$, CuO: % decline $r_c/r_o = 0.063^*$fv/fm, $r^2 = 0.48$).

Huntsman, 1998). Within the cell, redox active metal free ions can mediate the formation of toxic reactive oxygen species (e.g., hydroxyl radicals via Fenten chemistry) and reactive metals such as Cu and Zn can adventitiously bind with protein coordination sites or displace nutrient metals from their active sites in metalloproteins (Hartwig, 2001; Valko et al., 2005). In response, cells sequester excess metals to prevent such toxicity (Finney and O'Halloran, 2003), although these mechanisms have limits (Masmoudi et al., 2013). For example, algal cells may produce phytochelatins (PC), cystein-rich pseudopeptides that chelate various metals, including Cd, Cu and Zn (Branco et al., 2010). To minimize this production of ROS, photosynthetic organisms can activate several systems that may involve proline, ascorbate, or carotenoid pigments (Bertrand and Poirier, 2005). Such defense mechanisms may limit the ability of some cellular assays to effectively gauge metal toxicity.

The relevance of traditional effect statistics in toxicity testing for ecological risk assessment is questionable (Jager et al., 2006; Chapman et al., 1998). These statistics include the concentration at which a response variable or endpoint differs *x%* from the control, i.e., EC_x, where *x* commonly takes the value 0 (for the highest concentration not showing effect), 1, 5, 10 or 50%. Estimates for EC_x strongly depend on experimental design and choice of endpoint (Jager et al., 2006). Furthermore, while estimates for EC_{50} are typically robust (because these are located at the steepest point of the response curve), those of the ecologically more relevant EC_1, EC_5 and EC_{10} strongly depend on the functional form of the response curve and come with large confidence intervals. The shortcomings

outlined above can be overcome by using process-based models (Jager et al., 2006; Martin et al., 2013; Jager et al., 2011), such as that provided by the DEBtox framework, which combines a dynamic energy budget (DEB) model with models describing the toxicokinetic (TK) and toxicodynamic (TD) aspects of toxicant exposure (Muller et al., 2010).

While all ENPs tested showed a clear negative impact on the population growth rate of *I. galbana* (Fig. 1), none of the fluorescence-based HTS methods were able to consistently detect a signal forecasting an impact on growth. In fact, the responses to CuO, Ag, and ZnO ENP exposure never deviated more than 5% from the control in the HTS assays (Fig. S2-S5), though metals could be found in all cell fractions (Table 3). This is surprising, as transition metals typically invoke a broad spectrum of molecular responses, presumably including those for which the fluorescence-based HTS serve as indicators. It should be noted, however, that compensatory mechanisms may have mitigated the responses observable through our HTS techniques. For instance, in many eukaryotes, ROS levels are regulated within relatively tight margins, and only when the impact of an internal or external stressor exceeds the regulatory capacity of a cell will ROS levels increase sharply (Judson et al., 2013). Possibly, at sublethal exposure levels of our ENPs, compensatory processes were able to mask responses identifiable through HTS at the expense of a considerable amount of resources and, hence, influenced phytoplankton growth potential.

In contrast, all ENPs tested consistently reduced the efficiency of photosystem II (Figs. 2 and 3). This reflected our modeling results, which identified the model assuming toxic impact on assimilation, i.e., resource acquisition and processing, as the globally best performing toxico-dynamic model (see Table S1). Although there was a clear correlation between photosynthetic efficiency and population growth rate for all ENPs tested, the decline in population growth rate with decreasing photosynthetic efficiencies was much stronger in *I. galbana* exposed to ZnO and Ag ENMs than to CuO and CeO_2. This indicates that CuO and CeO_2 ENPs have a relatively strong negative impact on molecular processes other than those involved in determining photosynthetic efficiencies. Interestingly, this contrast between the two sets of ENPs was mirrored by the estimated values for the EC_{10} (with population growth rate as endpoint). These estimates were less than 1 mg L^{-1} for Ag (9.27 μM) and ZnO (12.3 μM) ENPs and more than 10 mg L^{-1} for CuO (125.7 μM) and CeO_2 (58.1 μM) (see Table 2). The relatively narrow 95% confidence intervals for the EC_{10} estimates clearly sets these two groups of ENPs apart and, importantly, show that the modeling approach developed here yield robust estimates of EC_x for low *x* values. The difference in impacts on photosynthetic yield and population growth between the two groups may be in part due to the solubility characteristics of the ENPs. Ag and ZnO ENPs dissolve readily compared to CuO ENPs, while CeO_2 ENPs are considered virtually insoluble (George et al., 2011). In sum, photosynthetic yield proved a reliable indicator for population level effects in our study, but it cannot be used quantitatively as a predictor of impact on population growth rates across nanomaterial species. An assessment of the quantitative impacts of exposure to ENPs and other nanomaterials at the population level would still require growth experiments.

HTS assays have been heralded as a key component of the future of ecotoxicological prediction and risk assessment (Collins et al., 2008; Hartung, 2009). There is no question that such approaches can have major advantages in scalability and rapidity (Nel et al., 2013). However, our results suggest that such an in vitro approach should proceed with caution and include organismal and population-level linkages. Traditional ecotoxicological testing is inherently reductionist: we often rely on a small group of model organisms that represent broad taxonomic groups that are incredibly diverse functionally and genetically, and study them in controlled conditions. In natural ecosystems, these organisms live in populations that interact with many other species in a complex and ever changing environmental matrix, and this may severely limit the relevance of such reductionist testing (Chapman, 2002; Chapman, 1995). Reducing these assessments even further, to the cellular level, and relying on only one or two model species to do so is likely an oversimplified approach to screening possible contaminants for environmental risk. HTS screens have utility for toxicological assessment of large numbers of chemicals and have proven useful to detect the most toxic compounds, especially with regards to human health (Forbes and Calow, 2012; Fernandes et al., 2009), and may pinpoint potential toxic mechanisms (George et al., 2011; George et al., 2010; Kwon et al., 2014). In bacteria, HTS assays of membrane integrity can be effective predictors of population growth effects (Priester et al., 2014). As we have shown here with regards to phytoplankton growth, photosynthetic efficiency can be a sensitive indicator of effects at larger biological scales and could itself be adopted as an HTS assay. However, wholesale adoption of such techniques and abandonment of more traditional ecotoxicological assays, such as population growth and mortality tests, would represent a step backward from our accumulated knowledge of toxicological effects on the environment. Instead, cellular screening should be guided by informed choice of endpoints given known toxicant characteristics, and the information used as part of a chain of knowledge or Adverse Outcome Pathway (AOP) that connects mechanistic data to endpoints meaningful to ecological impacts on individual organisms and populations (George et al., 2010; Forbes and Calow, 2012). These effects can in turn act in combination and potentially affect whole ecosystems in ways that are difficult to predict. We should embrace new technological approaches to toxicological risk assessment that allow examination of cellular and molecular process but this should not come at the expense of greater attention to the higher levels of biological organization, from the individual to populations and ecosystems.

Acknowledgements

Support was provided by the University of California Center for Environmental Implications of Nanotechnology, funded by the U.S. National Science Foundation and the Environmental Protection Agency under Cooperative Agreement Number DBI-0830117.

Appendix A. Supplementary data

Supplementary data associated with this article can be found, in the online version, at http://dx.doi.org/10.1016/j.aquatox.2016.12.009.

References

Barreto, J., O'Malley, W., Kubeil, M., Graham, B., Stephan, H., Spiccia, L., 2011. Nanomaterials applications in cancer imaging and therapy. Adv. Mater. 23 (12), H18–H40.
Bertrand, M., Poirier, I., 2005. Photosynthetic organisms and excess of metals. Photosynthetica 43 (3), 345–353.
Bielmyer-Fraser, G., Jarvis, T., Lenihan, H., Miller, R., 2014. Cellular partitioning of nanoparticulate versus dissolved metals in marine phytoplankton. Environ. Sci. Technol. 48 (22), 13443–13450.
Bowen, R., Depledge, M., 2006. Rapid assessment of marine pollution (RAMP). Mar. Pollut. Bull. 53 (10-12), 631–639.
Branco, D., Lima, A., Almeida, S., Figueira, E., 2010. Sensitivity of biochemical markers to evaluate cadmium stress in the freshwater diatom Nitzschia palea (Kutzing) W. Smith. Aquat. Toxicol. 99 (2), 109–117.
Chapman, P., Fairbrother, A., Brown, D., 1998. A critical evaluation of safety (uncertainty) factors for ecological risk assessment. Environ. Toxicol. Chem. 17 (1), 99–108.
Chapman, J., 1995. The role of ecotoxicity testing in assessing water-quality. Aust. J. Ecol. 20 (1), 20–27.
Chapman, P., 2002. Integrating toxicology and ecology: putting the eco into ecotoxicology. Mar. Pollut. Bull. 44 (1), 7–15.

Clijsters, H., Vanassche, F., 1985. Inhibition of photosynthesis by heavy-metals. Photosynth. Res. 7 (1), 31–40.
Collins, F., Gray, G., Bucher, J., 2008. Toxicology - transforming environmental health protection. Science 319 (5865), 906–907.
Edwards, M., Richardson, A., 2004. Impact of climate change on marine pelagic phenology and trophic mismatch. Nature 430 (7002), 881–884.
Fernandes, T., Diogo, M., Clark, D., Dordick, J., Cabral, J., 2009. High-throughput cellular microarray platforms: applications in drug discovery, toxicology and stem cell research. Trends Biotechnol. 27 (6), 342–349.
Finney, L., O'Halloran, T., 2003. Transition metal speciation in the cell: insights from the chemistry of metal ion receptors. Science 300 (5621), 931–936.
Forbes, V.E., Calow, P., 2012. Promises and problems for the new paradigm for risk assessment and an alternative approach involving predictive systems models. Environ. Toxicol. Chem. 31 (12), 2663–2671.
George, S., Pokhrel, S., Xia, T., Gilbert, B., Ji, Z., Schowalter, M., Rosenauer, A., Damoiseaux, R., Bradley, K., Madler, L., Nel, A., 2010. Use of a rapid cytotoxicity screening approach to engineer a safer zinc oxide nanoparticle through iron doping. ACS Nano 4 (1), 15–29.
George, S., Xia, T., Rallo, R., Zhao, Y., Ji, Z., Lin, S., Wang, X., Zhang, H., France, B., Schoenfeld, D., Damoiseaux, R., Liu, R., Lin, S., Bradley, K., Cohen, Y., Nal, A., 2011. Use of a high-throughput screening approach coupled with in vivo zebrafish embryo screening to develop hazard ranking for engineered nanomaterials. ACS Nano 5 (3), 1805–1817.
Godwin, H., Chopra, K., Bradley, K., Cohen, Y., Harthorn, B., Hoek, E., Holden, P., Keller, A., Lenihan, H., Nisbet, R., Nel, A., 2009. The university of california center for the environmental implications of nanotechnology. Environ. Sci. Technol. 43 (17), 6453–6457.
Gottschalk, F., Sonderer, T., Scholz, R., Nowack, B., 2009. Modeled environmental concentrations of engineered nanomaterials (TiO2, ZnO, Ag, CNT, fullerenes) for different regions. Environ. Sci. Technol. 43 (24), 9216–9222.
Gottschalk, F., Kost, E., Nowack, B., 2013. Engineered nanomaterials in water and soils: a risk quantification based on probabilistic exposure and effect modeling. Environ. Toxicol. Chem. 32 (6), 1278–1287.
Hanna, S., Miller, R., Muller, E., Nisbet, R., Lenihan, H., 2013a. Impact of engineered zinc oxide nanoparticles on the individual performance of *Mytilus galloprovincialis*. PLoS One 8 (4), e61800.
Hanna, S., Miller, R., Zhou, D., Keller, A., Lenihan, H., 2013b. Accumulation and toxicity of metal oxide nanoparticles in a soft-sediment estuarine amphipod. Aquat. Toxicol. 142, 441–446.
Hartung, T., 2009. Toxicology for the twenty-first century. Nature 460 (7252), 208–212.
Hartwig, A., 2001. Zinc finger proteins as potential targets for toxic metal ions: differential effects on structure and function. Antioxid. Redox Signal. 3 (4), 625–634.
Jager, T., Heugens, E., Kooijman, S., 2006. Making sense of ecotoxicological test results: towards application of process-based models. Ecotoxicology 15 (3), 305–314.
Jager, T., Albert, C., Preuss, T., Ashauer, R., 2011. General unified threshold model of survival – a toxicokinetic-toxicodynamic framework for ecotoxicology. Environ. Sci. Technol. 45 (7), 2529–2540.
Judson, R., Kavlock, R., Martin, M., Reif, D., Houck, K., Knudsen, T., Richard, A., Tice, R., Whelan, M., Xia, M., Huang, R., Austin, C., Daston, G., Hartung, T., Fowle, J., Wooge, W., Tong, W., Dix, D., 2013. Perspectives on validation of high-Throughput assays supporting 21 st century toxicity testing. ALTEX-Altern. Anim. Exp. 30 (1), 51–66.
Keller, A.A., Wang, H., Zhou, D., Lenihan, H.S., Cherr, G., Cardinale, B.J., Miller, R., Ji, Z., 2010. Stability and aggregation of metal oxide nanoparticles in natural aqueous matrices. Environ. Sci. Technol. 44 (6), 1962–1967.
Klaine, S., Alvarez, P., Batley, G., Fernandes, T., Handy, R., Lyon, D., Mahendra, S., McLaughlin, M., Lead, J., 2008. Nanomaterials in the environment: behavior, fate, bioavailability, and effects. Environ. Toxicol. Chem. 27 (9), 1825–1851.
Knudsen, T., Keller, D., Sander, M., Carney, E., Doerrer, N., Eaton, D., Fitzpatrick, S., Hastings, K., Mendrick, D., Tice, R., Watkins, P., Whelan, M., FutureTox, I.I., 2015. In vitro data and In silico models for predictive toxicology. Toxicol. Sci. 143 (2), 256–267.
Kwon, S., Lee, D., Shah, D., Ku, B., Jeon, S., Solanki, K., Ryan, J., Clark, D., Dordick, J., Lee, M., 2014. High-throughput and combinatorial gene expression on a chip for metabolism-induced toxicology screening. Nat. Commun., 5.
Lucas, A., Dupont, C., Tai, V., Largier, J., Palenik, B., Franks, P., 2011. The green ribbon: multiscale physical control of phytoplankton productivity and community structure over a narrow continental shelf. Limnol. Oceanogr. 56 (2), 611–626.
Marchetti, A., Parker, M., Moccia, L., Lin, E., Arrieta, A., Ribalet, F., Murphy, M., Maldonado, M., Armbrust, E., 2009. Ferritin is used for iron storage in bloom-forming marine pennate diatoms. Nature 457 (7228), 467–470.
Martin, B., Jager, T., Nisbet, R., Preuss, T., Hammers-Wirtz, M., Grimm, V., 2013. Extrapolating ecotoxicological effects from individuals to populations: a generic approach based on Dynamic Energy Budget theory and individual-based modeling. Ecotoxicology 22 (3), 574–583.
Masmoudi, S., Nguyen-Deroche, N., Caruso, A., Ayadi, H., Morant-Manceau, A., Tremblin, G., Bertrand, M., Schoefs, B., 2013. Cadmium, copper, sodium and zinc effects on diatoms: from heaven to hell – A review. Cryptogamie Algologie 34 (2), 185–225.
Mauter, M., Elimelech, M., 2008. Environmental applications of carbon-based nanomaterials. Environ. Sci. Technol. 42 (16), 5843–5859.
Merchant, S., 2010. The elements of plant micronutrients. Plant Physiol. 154 (2), 512–515.
Miller, R., Lenihan, H., Muller, E., Tseng, N., Hanna, S., Keller, A., 2010. Impacts of metal oxide nanoparticles on marine phytoplankton. Environ. Sci. Technol. 44 (19), 7329–7334.
Montes, M., Hanna, S., Lenihan, H., Keller, A., 2012. Uptake, accumulation, and biotransformation of metal oxide nanoparticles by a marine suspension-feeder. J. Hazard. Mater. 225, 139–145.
Muller, E., Nisbet, R., Berkley, H., 2010. Sublethal toxicant effects with dynamic energy budget theory: model formulation. Ecotoxicology 19 (1), 48–60.
Nel, A., Xia, T., Meng, H., Wang, X., Lin, S., Ji, Z., Zhang, H., 2013. Nanomaterial toxicity testing in the 21st century: use of a predictive toxicological approach and high-throughput screening. Acc. Chem. Res. 46 (3), 607–621.
Pitkethly, M., 2004. Nanomaterials – the driving force. Mater. Today 7 (12), 20–29.
Priester, J.H., Singhal, A., Wu, B., Stucky, G.D., Holden, P.A., 2014. Integrated approach to evaluating the toxicity of novel cysteine-capped silver nanoparticles to Escherichia coli and Pseudomonas aeruginosa. Analyst 139 (5), 954–963.
Rao, C.N.R., Müller, A., Cheetham, A.K., 2004. The Chemistry of Nanomaterials: Synthesis, Properties and Applications. Wiley-VCH, Weinheim.
Sunda, W., Huntsman, S., 1995. Iron uptake and growth limitation in oceanic and coastal phytoplankton. Mar. Chem. 50 (1–4), 189–206.
Sunda, W., Huntsman, S., 1996. Antagonisms between cadmium and zinc toxicity and manganese limitation in a coastal diatom. Limnol. Oceanogr. 41 (3), 373–387.
Sunda, W., Huntsman, S., 1998. Interactions among Cu2+, Zn2+, and Mn2+ in controlling cellular Mn, Zn, and growth rate in the coastal alga Chlamydomonas. Limnol. Oceanogr. 43 (6), 1055–1064.
Thio, B.J.R., Montes, M.O., Mahmoud, M.A., Lee, D.W., Zhou, D., Keller, A.A., 2011. Mobility of capped silver nanoparticles under environmentally relevant conditions. Environ. Sci. Technol. 46 (13), 6985–6991.
Valko, M., Morris, H., Cronin, M., 2005. Metals, toxicity and oxidative stress. Curr. Med. Chem. 12 (10), 1161–1208.
West, J., Halas, N., 2003. Engineered nanomaterials for biophotonics applications: improving sensing, imaging, and therapeutics. Annu. Rev. Biomed. Eng. 5, 285–292.

Table SI.1. Log likelihood and parameter values for 3 TD models; estimated values have 95% confidence intervals.

	Ag		CeO2		ZnO		CuO	
	Estimate	95% CI	Estimate	95% CI	Estimate	95% CI	Estimate	95% CI
effect on maintenance and assimilation			No convergence					
ln L	-93.52				-270.8		-226.1	
N_0 (cells µl^{-1})	32.92	[30.6-35.4]			40.22	[29.4-54.4]	6.56	[5.95-7.23]
r_0 (day^{-1})	1.24	[1.20-1.28]			0.71	[0.36-0.82]	1.31	[1.27-1.35]
EC_{10} (µM)	11.0	[8.53-14.7]			3.58	[2.58-6.14]	148	[95.4-233]
C_0 (µM)	0	-			2.93	[1.84-6.02]	0	-
C_k (µM)	57.9	[46.5-76.0]			6.10	[3.81-9.46]	600	[319->1e4]
effect on assimilation			No convergence					
ln L	-89.26				-264.2		-226.1	
N_0 (cells µl^{-1})	32.86	[30.6-35.3]			43.83	[31.1-61.8]	6.56	[5.95-7.23]
r_0 (day^{-1})	1.26	[1.22-1.31]			0.66	[0.54-0.78]	1.31	[1.27-1.35]
EC_{10} (µM)	7.23	[4.91-10.8]			6.11	[5.53-7.49]	150	[96.1-231]
C_{E0} (µM)	0	-			5.87	[5.16-7.37]	0	-
C_{Ek} (µM)	14.7	[9.46-24.0]			3.00	[1.23-5.90]	337	[80.1>1e4]
effect on maintenance								
ln L	-115.3		-178.05		-311.1		-227.0	
N_0 (cells µl^{-1})	32.86	[30.0-36.0]	31.25	[29.1-33.5]	43.83	[26.4-72.8]	6.56	[5.94-7.24]
r_0 (day^{-1})	1.19	[1.15-1.23]	0.97	[0.95-1.00]	0.53	[0.37-0.89]	1.30	[1.26-1.34]
EC_{10} (µM)	35.2	[31.0-41.0]	94.5	[74.4-131]	6.51	[<0-8.60]	175	[141-234]
C_{M0} (µM)	0	-	0	-	-0.12	[-23.2-2.83]	0	-

Supplemental figure legends

Fig. S1. Growth of *Isochrysis galbana* exposed to (A) Ag, (B) CeO_2, (C) ZnO and (D) CuO nanomaterials at nominal concentrations ranging from 0 to 20 ppm (see top table for color coding). Data represent means from 4-5 replicates. Lines represent model fits to data. The model is Equation SI.3 with SI.11 (Ag, ZnO and CuO) or SI.12 (CeO_2); for parameter estimates, see Table 2 in the main text. Initial cell densities are target values rather than measurements, and were therefore not included in the fitting procedure. Also, measurements beyond day 4 were excluded from the fitting procedure, as cultures had passed the exponential growth phase. Note that when data and fits are plotted on top of one another, the color representing the highest exposure level takes precedence; for instance, in panel C, the black curve is hidden under the red curve.

Fig. S2. Membrane permeability of *Isochrysis galbana* in response to increasing concentration of metal oxide ENPs, expressed relative to control cultures. Multiple lines and symbols on each plot represent response at successive times (24, 48, and 72 hr).

Fig. S3. Mitochondrial membrane potential of *Isochrysis galbana* in response to increasing concentration of metal oxide ENPs, expressed relative to control cultures. Multiple lines and symbols on each plot represent response at successive times (24, 48, and 72 hr).

Fig. S4. Intracellular ROS production in *Isochrysis galbana* in response to increasing concentration of metal oxide ENPs, expressed relative to control cultures. Multiple lines and symbols on each plot represent response at successive times (24, 48, and 72 hr).

Fig. S5. Calcein AM fluorescence, and indicator of ABC transport function, in *Isochrysis galbana* in response to increasing concentration of metal oxide ENPs, expressed relative to control cultures. Multiple lines and symbols on each plot represent response at successive times (24, 48, and 72 hr).

Fig. S1

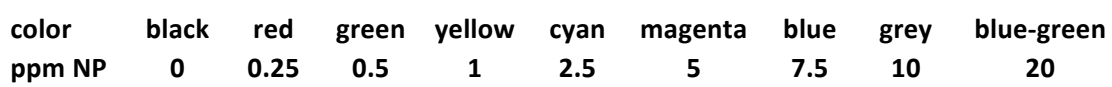
color black red green yellow cyan magenta blue grey blue-green
ppm NP 0 0.25 0.5 1 2.5 5 7.5 10 20

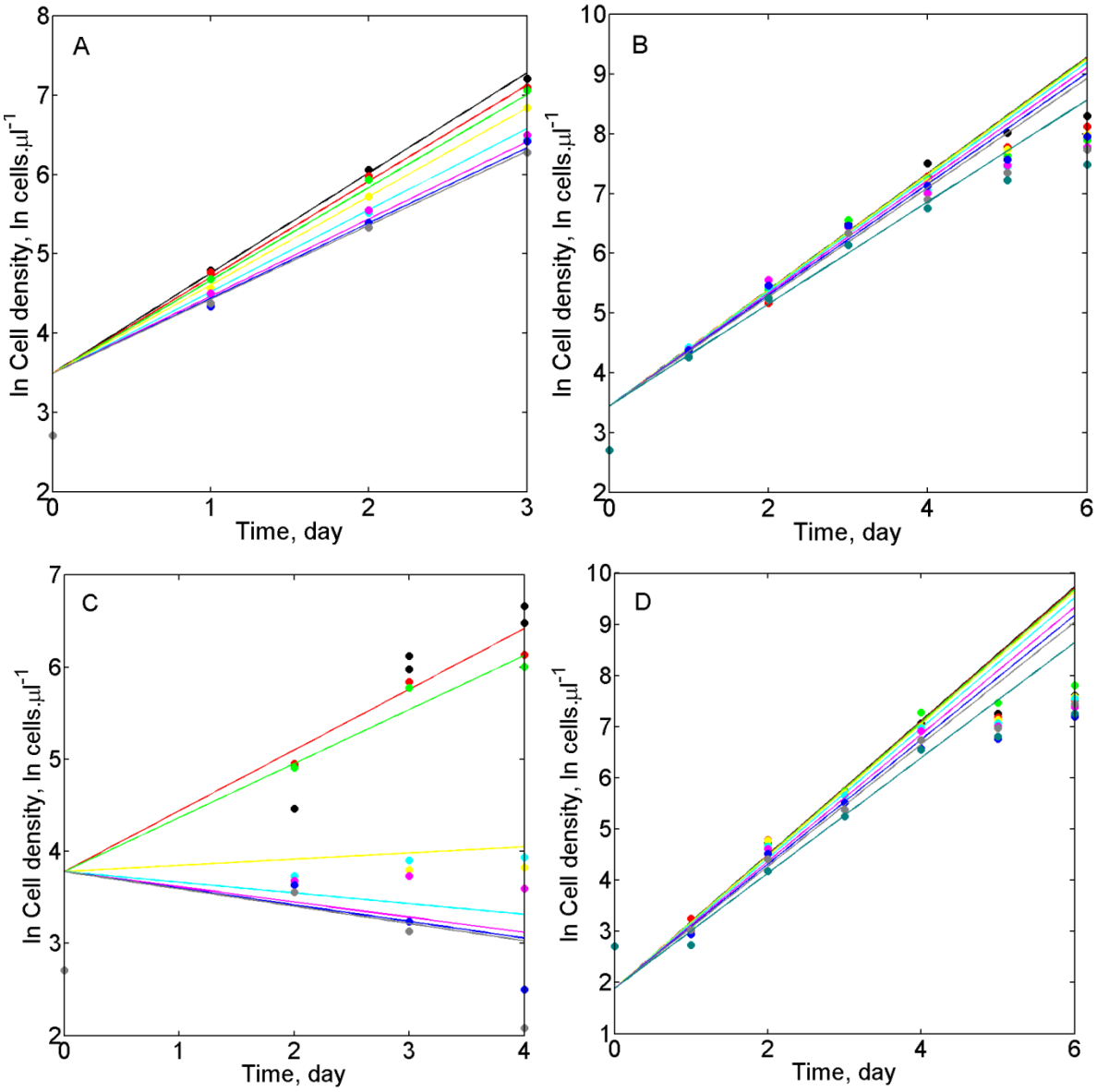

Fig. S2.

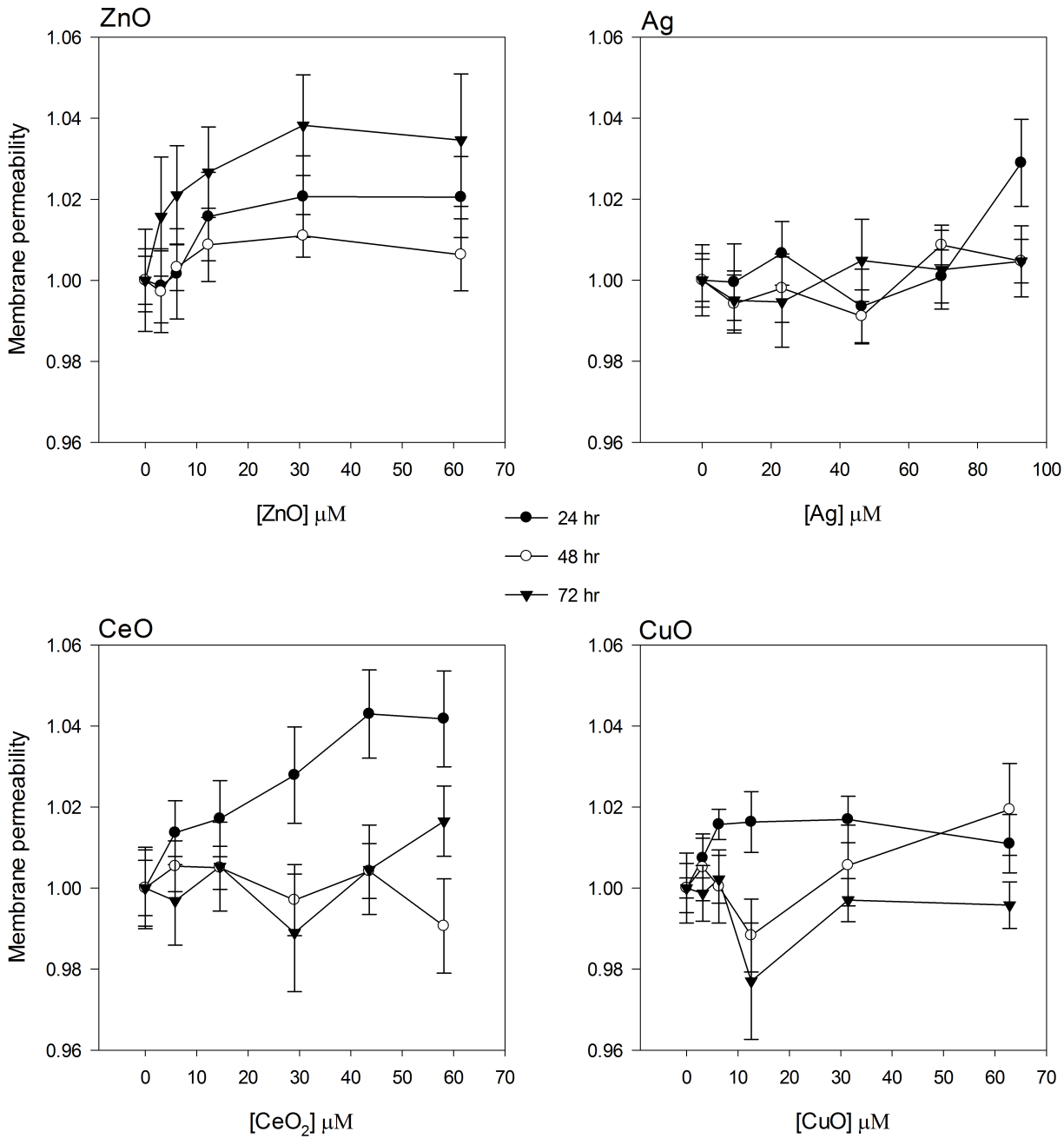
ZnO
Ag
CeO
CuO
Membrane permeability
[ZnO] μM
[Ag] μM
[CeO2] μM
[CuO] μM
24 hr
48 hr
72 hr

61

62 Fig. S3

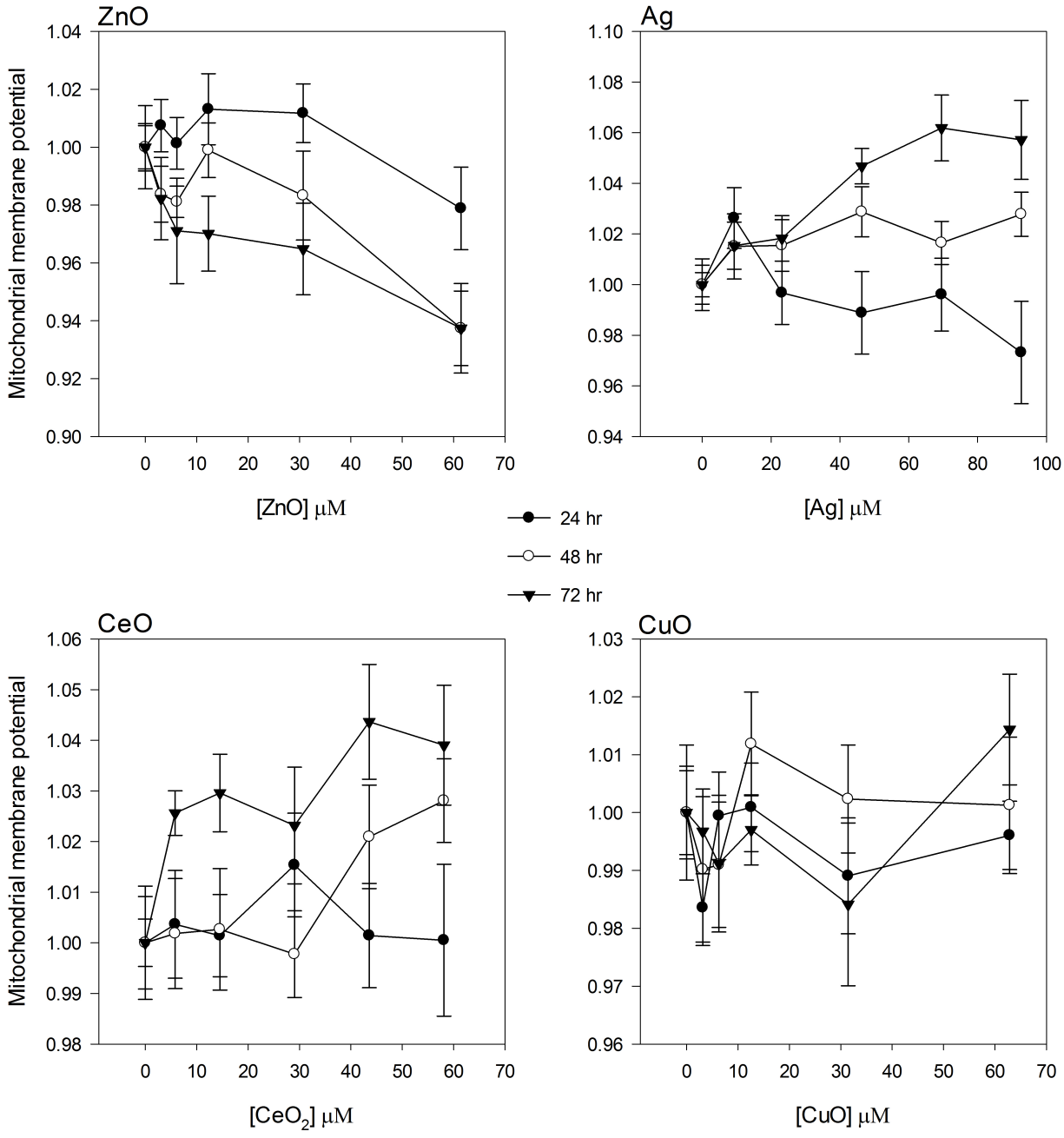

63

64

Fig. S4

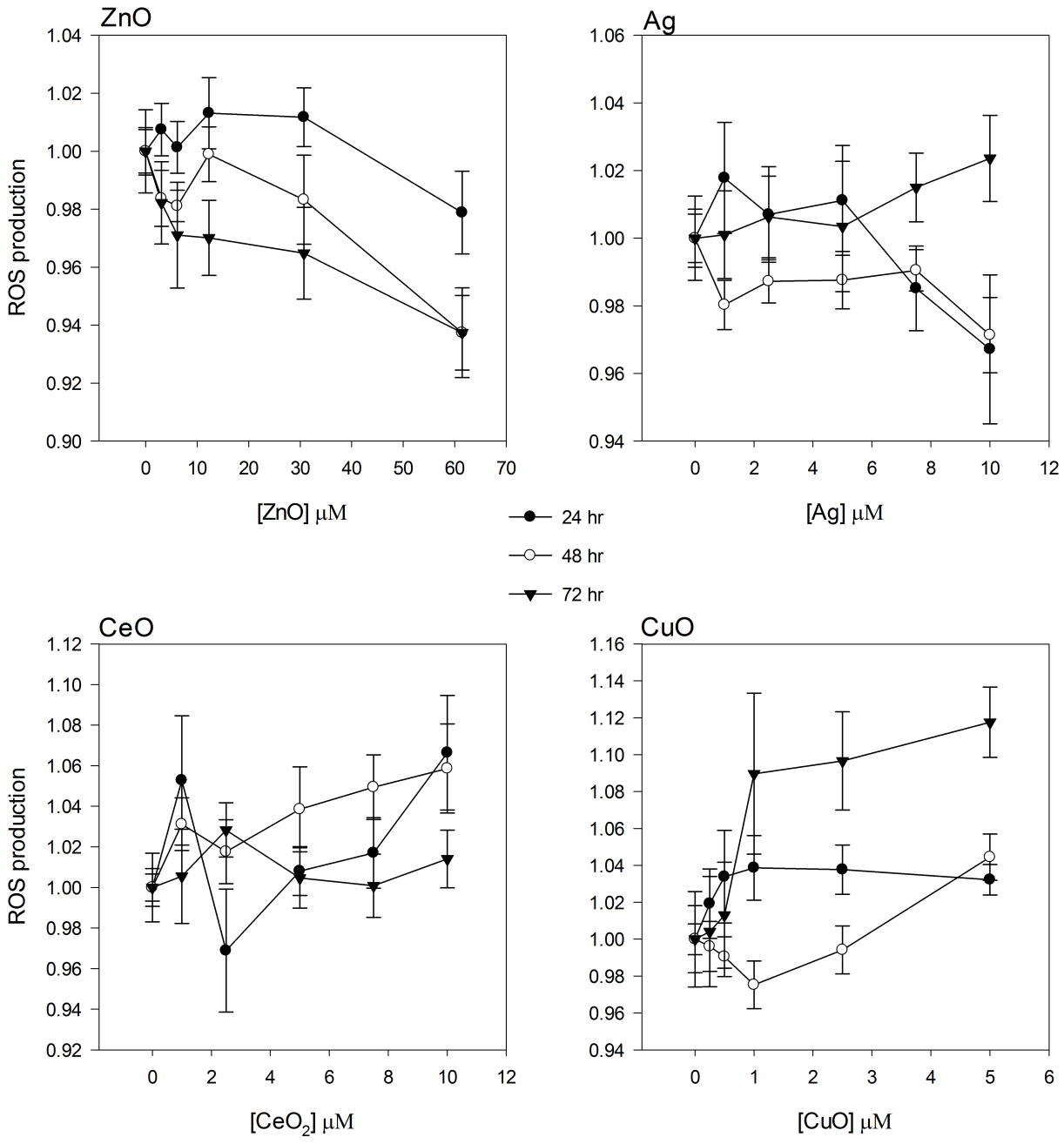
ZnO
Ag
CeO
CuO
ROS production
[ZnO] μM
[Ag] μM
[CeO2] μM
[CuO] μM
24 hr
48 hr
72 hr

69 Fig. S5.

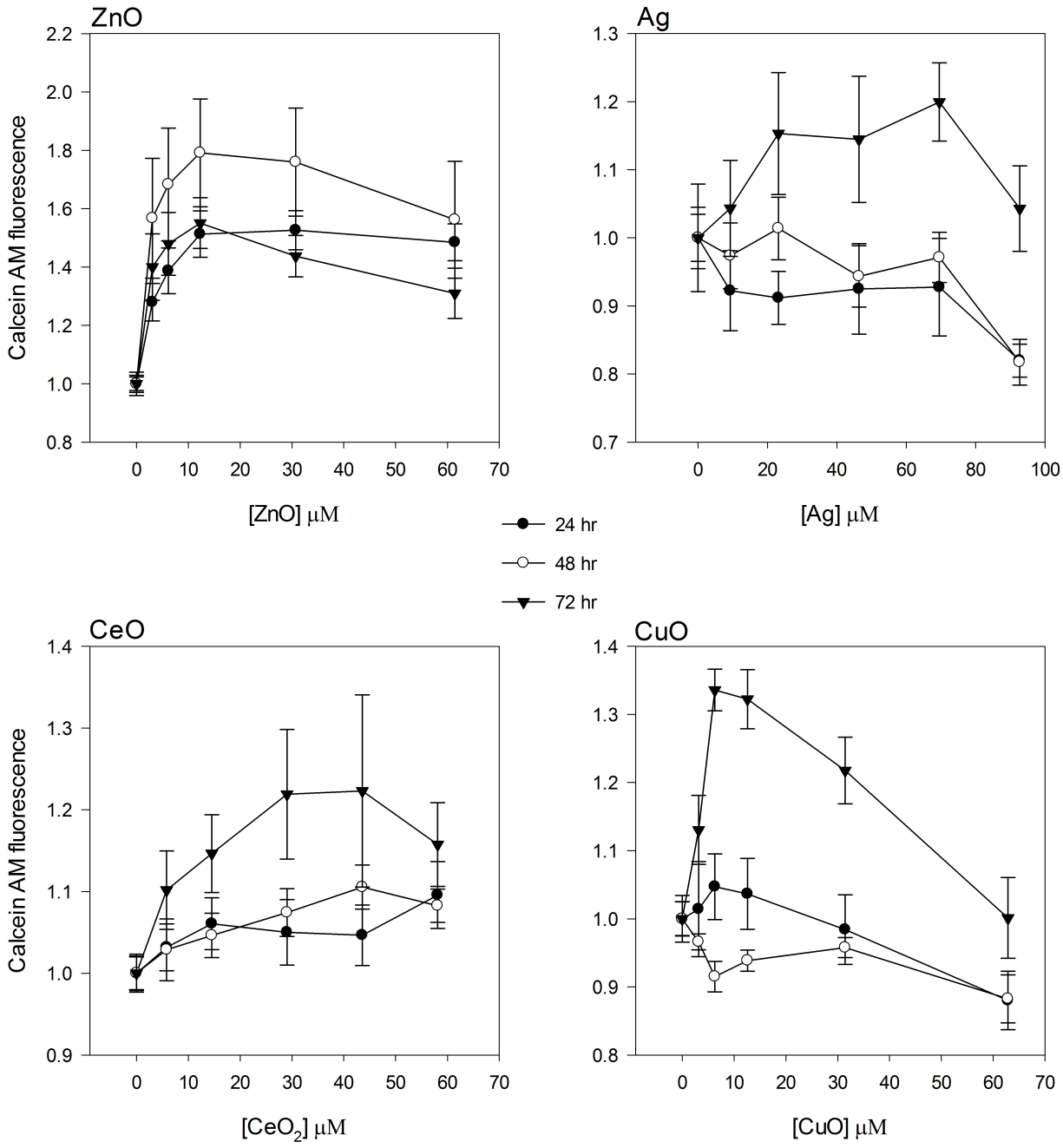
ZnO
Ag
CeO
CuO
Calcein AM fluorescence
[ZnO] μM
[Ag] μM
[CeO2] μM
[CuO] μM
24 hr
48 hr
72 hr

70

SUPPLEMENTAL INFORMATION

Dynamic Energy Budget (DEB) theory describes the population dynamics of dividing unicellular organisms with a constant structural biomass to cell surface area with two state equations for the cell density and the scaled reserve density [1-3]:

$$\frac{dN}{dt} = r_C N \text{ with } r_C = \frac{k_{E,C} e - k_{M,C} g}{e + g} \quad \text{(SI.1)}$$

and

$$\frac{de}{dt} = \left(f - e\right) k_{E,C} \quad \text{(SI.2)}$$

in which N is the cell density; r_C is the population growth rate (a subscripted 'C' means the quantity is potentially subject to toxicant effect); e is the scaled energy reserve density; $k_{E,C}$ is the assimilation rate parameter in the presence of toxicants; $k_{M,C}$ is the maintenance rate in the presence of toxicants; g is the growth investment; and f is the scaled functional response. We use the term "assimilation" to characterize the integrated physiological processes involved in production of energy reserves, and define "functional response" to be the ratio of the rate of production of energy reserves to its maximum value with unlimited light and nutrients.

We assume that in our experiments, resources are abundant, so $f = 1$. We further assume that at, or soon after, the start of the experiments energy reserve density has stabilized; Equation SI.2 then implies that $e = f$, which effectively eliminates the scaled reserve density as a dynamic quantity. This leaves Equation SI.1 as the sole state equation needed to describe population dynamics, which has the solution

$$\ln N_{t,C} = \ln N_{0,C} + r_C t \quad \text{(SI.3)}$$

with

$$r_C = \frac{k_{E,C} - k_{M,C} g}{1+g} \tag{SI.4}$$

and $N_{0,C}$ as the initial cell density at exposure concentration C.

If toxicants are exchanged rapidly relatively to the population growth rate and experimental duration, the impact of toxicants can directly be related to the exposure concentration. Defining the toxicodynamic effect functions for assimilation and maintenance, f_E and f_M , respectively, via

$$f_* = 1 + \frac{\left(C - C_{*0}\right)_+}{C_{*k}} \tag{SI.5}$$

with * representing *'E'* or '*M'*, and C_{*0} and C_{*k} as the no-effect concentration and the toxic effect scaling parameter, respectively (the subscripted '+' indicates that $C - C_{*0} = 0$ if $C \le C_{*0}$). Substitution of the toxic effect functions in Equation SI.4 yields

$$r_C = \frac{\frac{k_E}{f_E} - k_M f_M g}{1+g} \tag{SI.6}$$

in which k_E and k_M are the reserve turn-over and maintenance rates in the absence of toxicants.

The bioenergetic parameters k_E, k_M and g in Equation SI.6 cannot be estimated from data of cell densities in the exponential growth phase alone. However, they can be eliminated by defining $p \equiv k_M g \left(1+g\right)^{-1}$ and $r_0 \equiv \left(k_E - k_M g\right)\left(1+g\right)^{-1}$. The former is a compound parameter of no special significance, and will be eliminated below; the latter is the maximum population growth rate with abundant resources and without toxicant exposure. With a little algebraic manipulation, Equation SI.6 can be written as

$$r_C = \frac{k_E - k_M g + k_M g}{f_E\left(1+g\right)} - \frac{k_M f_M g}{1+g} = \frac{r_0}{f_E} - p\left(f_M - \frac{1}{f_E}\right) \tag{SI.7}$$

Of special interest in ecotoxicological risk assessment is EC_X, the exposure concentration that causes X % reduction in the population growth rate. Here it is more convenient to work with fractions and use remaining functionality as vantage point. Let $x = 1 - 0.01X$, $r_x \equiv xr_0$ and, to retain notational consistency, $C_X \equiv \mathrm{EC_X}$. Furthermore, when $C = C_X$, let $f_E = f_{EX}$ and $f_M = f_{MX}$. Then, from Equation SI.7,

$$r_x = \frac{r_0}{f_{EX}} - p\left(f_{MX} - \frac{1}{f_{EX}}\right) \tag{SI.8}$$

or

$$p = \frac{(r_0 - r_x f_{EX})}{(f_{EX} f_{MX} - 1)} = \frac{r_0 (1 - x f_{EX})}{(f_{EX} f_{MX} - 1)} \tag{SI.9}$$

Substitution of Equation SI.9 into SI.7 gives

$$r_C = \frac{r_0}{f_E}\left(1 - \frac{(1 - x f_{EX})(f_E f_M - 1)}{(f_{EX} f_{MX} - 1)}\right) \tag{SI.10}$$

This expression can be written in terms of the exposure concentration, but the result is not illuminating.

Three special cases are particularly useful: toxic effects on assimilation and maintenance are scaled similarly ($f_E = f_M$ and thus $f_{EX} = f_{MX}$); toxicant exposure leads to impact on assimilation only ($f_{MX} = f_M = 1$); and toxicant exposure leads to impact on maintenance only ($f_{EX} = f_E = 1$). In the latter two special cases, it makes sense to express Equation SI.10 in terms of the exposure concentration. If only assimilation is affected by a toxicant,

$$r_C = \frac{r_0 C_{Ek}}{C_{Ek} + (C - C_{E0})_+}\left(1 - \frac{(C - C_{E0})_+}{(C_x - C_{E0})_+}\left(1 - x\left(1 + \frac{(C_x - C_{E0})_+}{C_{Ek}}\right)\right)\right) \tag{SI.11}$$

which is a decelerating function of exposure concentrations beyond the no-effect concentration. With toxicant impact on maintenance only,

$$r_C = r_0\left(1-\frac{(1-x)}{(C_x-C_{M0})_+}(C-C_{M0})_+\right) \quad \text{(SI.12)}$$

in which the population growth rate decreases linearly with exposure concentrations beyond the no-effect concentration. Note that with toxicant impact on assimilation only, Equation SI.11 may reduce to a form that is functionally similar to Equation SI.12, since

$$\begin{aligned}\lim_{C_{Ek}\to\infty}\frac{r_0 C_{Ek}}{C_{Ek}+(C-C_{E0})_+}&\left(1-\frac{(C-C_{E0})_+}{(C_x-C_{E0})_+}\left(1-x\left(1+\frac{(C_x-C_{E0})_+}{C_{Ek}}\right)\right)\right)\\ &= r_0\left(1-\frac{(1-x)}{(C_x-C_{E0})_+}(C-C_{E0})_+\right)\end{aligned} \quad \text{(SI.13)}$$

In practice, this means that if the highest toxicant exposure level is lower than C_{Ek}, it will be difficult to estimate the latter from growth data, while it will be hard to discern impact on assimilation from that on maintenance in growth data.

References

1. Kooijman, S. A. L. M., *Dynamic energy and mass budgets in biological systems*. 3rd ed.; Cambridge University Press: Cambridge, 2010.

2. Miller, R. J.; Lenihan, H. S.; Muller, E. B.; Tseng, N.; Hanna, S. K.; Keller, A. A., Impacts of Metal Oxide Nanoparticles on Marine Phytoplankton. *Environmental Science & Technology* **2010,** *44*, (19), 7329-7334.

3. Muller, E. B.; Anathasubramaniam, B.; Klansjeck, T.; Nisbet, R. M., Entrainment of cell division in phytoplankton with dynamic energy budgets. *J. Sea. Res.* **2011,** *66*, 447-455.